Journal of Intelligent Material Systems and Structures

Original Article

Journal of Intelligent Material Systems and Structures
1–12

DOI: 10.1177/1045389X211023583
journals.sagepub.com/home/jim
SAGE

A rate-dependent KP modeling and direct compensation control technique for hysteresis in piezo-nanopositioning stages

Rui Xu[1], Dapeng Tian[1] and Miaolei Zhou[2]

Abstract

This paper first presents a rate-dependent Krasnosel'skii-Pokrovskii (RKP) model to capture the hysteresis of piezo-nanopositioning stages. The dynamic density function of the RKP model is obtained via neural network with frequency behavior input signal. Under the persistently exciting condition, the convergence of the neural network with Krasnosel'skii-Pokrovskii (KP) operators is proved rigorously. In order to address the hysteresis issue, a direct compensation control (DCC) approach with the KP compensation operator is proposed, where its dynamic density function is same as that of the RKP model. Some experiments with different reference signals are conducted to verify the effectiveness of the proposed modeling and DCC method on piezo-nanopositioning stages.

Keywords

Hysteresis, Krasnosel'skii-Pokrovskii model, piezo-nanopositioning stage, persistently exciting

1. Introduction

Owing to the advantages of high-frequency response, ultrahigh resolution, large stiffness and few hot, piezo-nanopositioning stages are widely adopted as nanopositioning equipments (Chen et al., 2016; Dong et al., 2016). However, some nanopositioning stages based on piezoelectric materials display complex rate-dependent hysteresis, which makes their application quite challenging (Nguyen et al., 2018; Zhang et al., 2019). When the frequency of the input signal increases, the width of the hysteresis loop increases and the stroke of piezo-nanopositioning stages decreases. To describe and mitigate the complex hysteresis of nanopositioning stages, many modeling and control approaches have been investigated in existing literatures (Yu et al., 2021).

The existing hysteresis models are classified into three categories: differential-equation-type (DET) hysteresis model, operator-type (OT) hysteresis model and other machine learning (ML) hysteresis model. The DET hysteresis model is proposed via a first-order nonlinear differential equation to reveal the mapping relationship between the input and output, which mainly includes the Bouc-Wen model (Xu and Zhou, 2017a), Duhem model (Zhou et al., 2016) and Jiles-Atherton model (Liu et al., 2016), etc. However, the traditional DET hysteresis model does not have the rate-dependent characteristic, which causes modeling accuracy deteriorated to accommodate the input frequency changes. To make the traditional DET hysteresis model have the rate-dependent characteristic, the dynamical model of nanopositioning stages is built to compose a Class-Hammerstein hysteresis model with rate-dependent characteristic (Guo et al., 2015). It is shown that such modeling approach needs to understand the structure of nanopositioning stages, which requires abundant electronics and machinery knowledge and makes the hysteresis modeling more difficult. The frequently-used OT hysteresis model includes Preisach model (Iyer et al., 2005; Tan and Baras, 2005), Prandtl-Ishlinskii (PI) model (Zhang et al., 2015) and Krasnosel'skii-Pokrovskii (KP) model (Li et al., 2018; Xu and Zhou, 2017b), etc. They are obtained via the accumulated hysteresis operators on Preisach plane. For instance, the

[1]Key Laboratory of Airborne Optical Imaging and Measurement, Changchun Institute of Optics, Fine Mechanics and Physics, Chinese Academy of Sciences, Changchun, Jilin, China
[2]Department of Control Science and Engineering, Jilin University, Changchun, Jilin, China

Corresponding author:
Miaolei Zhou, Department of Control Science and Engineering, Jilin University, Changchun, Jilin 130022, China.
Email: zml@jlu.edu.cn

Preisach model is formed by the summation of Preisach operators with different weights, which simply describes the symmetric hysteresis loop. The PI model is composed of the Play or Stop operators, which is more accurate to describe the hysteresis loop of the piezo-nanopositioning stages. Al Janaideh et al. (2021) adopted an adaptive identification algorithm to obtain the play radii of the a PI operator, to improve the accurate modeling of the hysteresis in smart material actuators. The KP model is built by a superposition of KP operators with density function, which not only can capture the asymmetrical hysteresis loop, but also can describe the major and minor hysteresis loops. Different from the Preisach model, the KP model has the continuity mapping space, and it requires less KP operators and reduces the computational burden. In addition, the KP model can describe the hysteresis effects with saturation. So, the KP model has more superior performance than other OT hysteresis models. Nevertheless, the traditional OT hysteresis model cannot describe the rate-dependent hysteresis characteristic. To solve this issue, some rate-dependent Preisach and PI models have been developed. For example, Xiao and Li (2012) proposed a rate-dependent Preisach model by linear superposition of the frequency weight and the density function. Yang et al. (2015)introduced a dynamic envelope function into the input function of the play or stop operators, and a rate-dependent PI model was established. In addition, Al Janaideh et al. (2020) proposed temperature-dependent PI model to capture the hysteresis nonlinearities of the piezoelectric actuator. The temperature shape function and the weights are obtained by the Grey Wolf Optimizer, the experimental results demonstrate that the proposed model can account for the temperature-dependent and hysteresis of the piezoelectric actuator. However, so far there has been few studies on the rate-dependent Krasnosel'skii-Pokrovskii (RKP) model. In this study, we have built a RKP model to describe rate-dependent hysteresis of piezo-nanopositioning stages.

These hysteresis models are commonly used to capture the hysteresis of nanopositioning stages. How to eliminate their hysteresis and improve the positioning accuracy is a key problem for realizing the application of nanopositioning stages in the precision drive field. In existent research literatures, inversions of the Preisach model and PI model were obtained to compensate the hysteresis of smart material actuators. Hu et al. (2005) designed a new inverse algorithm based on the inverse dynamic Preisach model to mitigate the hysteresis of the piezoceramic actuator. Song et al. (2005) proposed an inverse Preisach model to compensate the hysteresis of the piezoceramic actuator. To eliminate the hysteretic and creep effects in the piezoelectric actuator, a new compensator based on the Preisach approach was designed by Kuhnen and Krejci (2009), and it can be implemented in a real-time way. Due to the inverse Preisach model obtained by the numerical algorithm, it increased the computational burden. The inverse PI model was obtained via the relationship between the play operator and stop operator and it was easier to be obtained than the inverse Preisach model. For example, Al Janaideh and Krejci (2012) adopted an inverse rate-dependent PI model to design a feedforward controller for piezo-micropositioning actuators. Compared with the Preisach model and PI model, the KP model requires fewer operators to describe a same hysteresis loop (Li et al., 2018). In the existing literature (Webb et al., 1998), the only way to gain the inverse of the KP model was the recursive method, but this method had no special advantages in computational cost compared with other hysteresis models.

In this paper, we make use of the advantages of KP model in describing the asymmetrical major and minor hysteresis loop. The rate-independent characteristic of the KP operator is analyzed theoretically. Next, to establish RKP model and capture the dynamic hysteresis, the derivative of the input voltage signal is used as the input of neural network to obtain the dynamic density function with persistently exciting input signals. The convergence property of the neural network with KP operators is demonstrated under the persistently exciting conditions of the input. In order to deal with the hysteresis issue, we design a direct compensation control (DCC) by analyzing the structure of RKP model for the hysteresis in the piezo-nanopositioning stage. Experimental results are provided to demonstrate the effectiveness of the proposed RKP model and DCC method on the piezo-nanopositioning stage.

The main contributions of this paper are as follows:

(1) The RKP model is first designed and we just use ten KP operators to accurately capture the rate-dependent hysteresis of the piezo-nanopositioning stage and it reduces the computational consumption of the hysteresis modeling.
(2) The convergence of the neural network for obtaining the dynamic density function of the RKP model is proved theoretically under the persistently exciting condition.
(3) A DCC technique is proposed to mitigate the impact of the hysteresis and achieve high-precision tracking control on the piezo-nanopositioning stage.

2. Recall of the Krasnosel'skii-Pokrovskii model

2.1. KP operator

Due to the ability of describing the major and minor hysteresis loops, the KP model is widely used to describe the hysteresis of smart material actuators. The KP model is composed of the KP operators and density

function. The KP operator is shown in Figure 1(a), and its equation is written as

$$\psi_{\nu_1,\nu_2}[u(t);\zeta(\nu_1,\nu_2)] = \begin{cases} \max[\zeta(\nu_1,\nu_2), r(u(t)-\nu_2)] & \dot{u}(t)>0 \\ \min[\zeta(\nu_1,\nu_2), r(u(t)-\nu_1)] & \dot{u}(t)\leqslant 0, \end{cases} \quad (1)$$

where $u(t)$ is the input voltage of the KP operator; $\psi_{\nu_1,\nu_2}[u(t);\zeta(\nu_1,\nu_2)]$ is the output of the KP operator, which is expressed as Γ_{kp} for the sake of simplicity. The (ν_1,ν_2) are a pair of thresholds of the Preisach plane $(\mathbf{P})$, which satisfies $\mathbf{P} = \{\mathbf{P}(\nu_1,\nu_2) \in \Re^2 : \nu_{\min} \leqslant \nu_1 \leqslant \nu_2 \leqslant \nu_{\max}\}$. The $\nu_{\min}$ and $\nu_{\max}$ are the boundary values of the Preisach plane. The $r(u(t);\nu_1,\nu_2)$ is the Lipschitz function, which influences the major loop shape of the KP operator. The formula of $r(u(t);\nu_1,\nu_2)$ is shown as

$$r(u(t);\nu_1,\nu_2) = \begin{cases} 0 & u(t)\in[-\infty,0] \\ \nu_{\max} * u(t)/\sigma & u(t)\in[0,\sigma] \\ \nu_{\max} & u(t)\in[\sigma,\ +\infty], \end{cases} \quad (2)$$

where $\sigma \in [0,\infty)$ is the slope of $r(u(t);\nu_1,\nu_2)$, which is calculated by $\sigma = 1/(L-1)$, L is the cutting line number of each axis on Preisach plane. $\zeta(\nu_1,\nu_2)$ is the previous maxima and minima value of the KP operator, which embodies the memory feature and is updated based on the input-output data of the KP operator. The $\zeta(\nu_1,\nu_2)$ is written as

$$\zeta(\nu_1,\nu_2)(t) = \begin{cases} 0 & t = T_0 \\ \Gamma_{\text{kp}}(t) & t = T_a \geqslant T_{a-1}, \dot{u}(t)\text{sgn}(\dot{u}(t))<0 \\ \zeta(\nu_1,\nu_2)(T_{a-1}) & t\in[T_{a-1},T_a], \dot{u}(t)\text{sgn}(\dot{u}(t))\geqslant 0, \end{cases} \quad (3)$$

where a is the times of the $\dot{u}(t)\text{sgn}(\dot{u}(t))<0$. According to (3), Γ_{kp} can record all previous extremum values. The KP model can describe the memory characteristic of hysteresis in smart material actuators. In addition, the KP operator is rate-independent, which meets the following Theorem 1.

Theorem 1. *Visintin (2013) If a continuous increasing function* $\varphi : [0,T] \to [0,T]$ *meets* $\varphi(0) = 0$ *and* $\varphi(T) = T$, *then for the* $u(t) \in C[0,T]$ *(*$C[0,T]$ *is the space of the continuous function on* $[0,T]$*),* $\chi[u\circ\varphi;x_0](t) = \chi[u(t);x_0](\varphi(t))$, $\forall\ t\in[0,T]$. *Then, the function* χ *is the rate-independent.*

According to the KP operator defined in (1), the KP model with the input $u(t)\in[u_{\min},u_{\max}]$ is expressed as

$$y(t) = \iint_P \psi_{\nu_1,\nu_2}[u(t);\zeta(\nu_1,\nu_2)]\varpi(\nu_1,\nu_2)d\nu_1 d\nu_2, \quad (4)$$

where $\varpi(\nu_1,\nu_2)$ is the density function of the KP model.

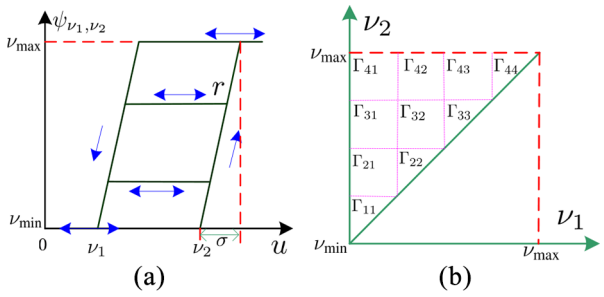

Figure 1. KP model: (a) KP operator and (b) Preisach plane with $L = 4$.

2.2. Discretization of the KP model

As shown in (4), the formula of the KP model is a double integral function. It is difficult to obtain the output of the KP model in the practical application. Thus, the KP model should be discretized in mathematical way. In this work, we assume that the KP operator is regarded as a cell on the discrete Preisach plane and the density function of the KP model is the constant. The discrete Preisach plane is obtained by dividing uniformly $\mathbf{P}$ into a mesh using L, which is given in Figure 1(b). The Preisach plane is divided into $N = L(L+1)/2$ cells. As $L\to\infty$, the discrete Preisach plane approximates to the continuous-Preisach plane. Then, each KP operator corresponds to each cell. We assume that the $[u_{\min},u_{\max}]\subseteq[\nu_{\min},\nu_{\max}]$ is the input maximum and minimum values of the KP operator. The discrete input levels of each axis are written as

$$\nu = \nu_{\min} + \frac{\nu_{\max}-\nu_{\min}}{L}(i-1), \quad (5)$$

where $i = 1,2,\cdots,L+1$. The smooth hysteresis curve is generated via the KP operator overlap cell by cell. The discrete KP model with the output y is expressed as

$$y = \sum_{i=1}^{L}\sum_{j=1}^{i}\Gamma_{\text{kp}}^{i,j}\varpi_{i,j}, \quad (6)$$

where $\Gamma_{\text{kp}}^{i,j}$ is the KP operator value of each cell on the Preisach plane, $\varpi_{i,j}$ denotes the density function of each KP operator after the discretization of the KP model. In this paper, we rewrite (6) as the normal discrete form of the linear systems for the convenience of obtaining the suitable density function and implementing the KP model, which is given as

$$y = \sum_{k=1}^{N}\Gamma_{\text{kp}}^{k}\varpi_k = \Gamma_{\text{kp}}^{T}\mathbf{w}, \quad (7)$$

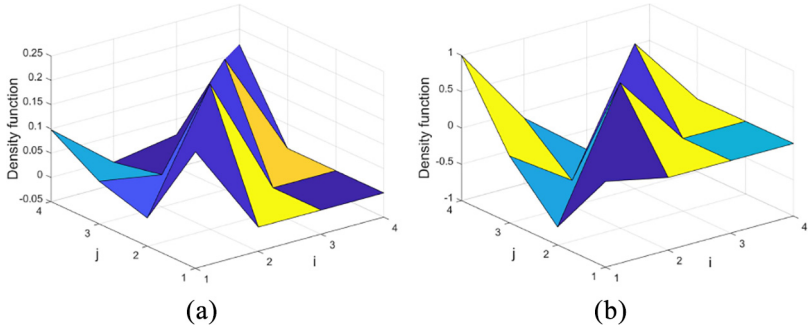

Figure 2. Density function of the KP model with different input frequencies: (a) 1 Hz and (b) 50 Hz.

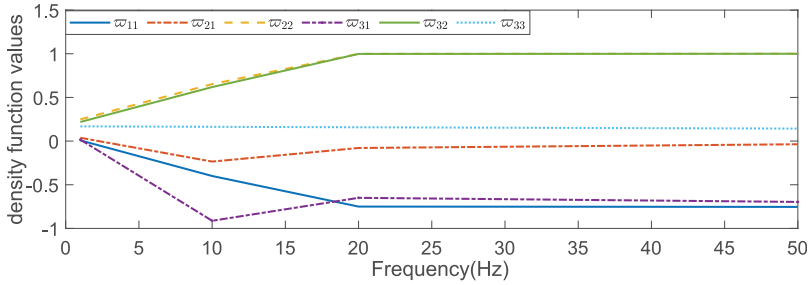

Figure 3. Relationship between the input frequency and density function value of the KP model.

where $\Gamma_{\mathrm{kp}} = [\Gamma_{11}\,\Gamma_{21}\,\Gamma_{22}\,\Gamma_{31}\,\Gamma_{32}\,\cdots\,\Gamma_{ij}\,\cdots\,\Gamma_{LL}]^T$, $\mathbf{w} = [\varpi_{11}\,\varpi_{21}\varpi_{22}\,\varpi_{31}\,\cdots\,\varpi_{ij}\,\cdots\,\varpi_{LL}]^T$.

3. Rate-dependent Krasnosel'skii-Pokrovskii model

3.1. Neural network identification method

In this section, the primary objective is to obtain an appropriate w to capture the hysteresis of the piezo-nanopositioning stage. As mentioned above, the hysteresis of the piezo-nanopositioning stage has the rate-dependent characteristic, but the KP operator can only describe the rate-independent hysteresis, not the rate-dependent hysteresis. There are two solutions to this problem. One is that we can design a RKP operator with the frequency information of the input signal to make the KP model have rate-dependent characteristic. However, designing a RKP operator requires complex mathematical calculations and it is different to be achieved in practice. The other is that we can build a RKP model with the dynamic density function of the KP model in real-time way. Because the output of the KP operator can be computed directly according to the input of the piezo-nanopositioning stage, we can use KP model with different density function (which is obtained based on the input frequency information) to describe the hysteresis loop at different frequency. The density function of the KP model at different input frequencies is shown in Figure 2. In this paper, we adopt the second method to build a RKP model.

As shown in Figure 3, the relationship between the input frequency and the density function of the KP model is complex nonlinear. It is difficult to describe the functional relationship between the input frequency and the density function. In this paper, we consider this relationship as the nonlinear mapping $\Re^{\vartheta} \rightarrow \Re^{y}$

$$Y = \mathbf{F}(\vartheta);\ Y \in \Re^{y},\ \vartheta \in \Re^{\vartheta}, \tag{8}$$

where ϑ is the input of the nonlinear mapping, Y is the output vector. Neural networks have the ability to approximate the nonlinear mappings based on the Lemma 1. Then Lemma 1 is given as follow.

Lemma 1. *Wang et al. (2017) The neural networks can approximate any nonlinear mappings* $\boldsymbol{F}(\cdot)$*:* $\Re^{\vartheta} \rightarrow \Re$ *with any compact set* $\Re^{\vartheta} \subset \Re^{q}$ *(q is the input dimension), which is given as*

$$\hat{Y} = \hat{\boldsymbol{F}}(\vartheta) + \boldsymbol{\epsilon} = \hat{\Theta}^T \Phi(\vartheta) + \boldsymbol{\epsilon}, \tag{9}$$

where $\hat{\Theta} \in \Re^{p}$ is the weight vector of the neural networks, $\| \boldsymbol{\epsilon} \| \leqslant \bar{\underline{\epsilon}}$ is the approximation error, $\Phi(\vartheta) \in [\phi_1(\vartheta), \phi_2(\vartheta), \cdots, \phi_m(\vartheta)]^T$ is the basis function

vector, $\bar{\epsilon}$ is the upper bound of ϵ. Assume that $\forall \vartheta \in \Re^{\vartheta} \subset \Re^{q}$, the optimal $\Theta^{\star}$ is existing with $\| \epsilon \| = \bar{\epsilon}$. $\Theta^{\star}$ is described as

$$\Theta^{\star} = arg \ min_{\hat{\Theta} \in \Re^{p}} \{ sup_{\vartheta \in \Re^{q}} | \hat{\Theta}^{T} \Phi(\vartheta) - \boldsymbol{F}(\vartheta) | \}. \quad (10)$$

In this paper, the structure diagram of the RKP model identification process is shown in Figure 4. $\dot{u}(t)$ represents the input frequency information and it is the input of the neural network, $\hat{\mathbf{w}}$ is the output of the neural network, which is used to replace and update the density function $\mathbf{w}$ of the RKP model. The function vector $\Phi(\cdot)$ constitutes the hidden layer, ϕ_i is the i th hidden layer node. The actual weight vector Θ of the output layer is given as

$$\Theta = [\theta_{11}, \cdots, \theta_{1m}; \theta_{21}, \cdots, \theta_{2m}; \cdots; \theta_{q1}, \cdots, \theta_{qm}]^{T} \quad (11)$$

This paper adopts the gradient method to obtain the weight parameters of the neural network, the modeling error is defined as

$$\begin{aligned} e(t) &= \hat{y}(t) - y(t) \\ &= \Gamma_{kp}^{T}(t) \hat{\Theta}^{T} \Phi(\dot{u}(t)) - \Gamma_{kp}^{T}(t) \Theta^{T} \Phi(\dot{u}(t)) - \epsilon \\ &= \Gamma_{kp}^{T}(t) (\hat{\Theta}^{T} - \Theta^{T}) \Phi(\dot{u}(t)) - \epsilon, \end{aligned} \quad (12)$$

where $\hat{y}(t)$ is the output of the RKP model. We define that the $\tilde{\Theta} = \hat{\Theta} - \Theta$ is the weight error of the neural network. The weight parameters updated using the gradient method is given as

$$\dot{\hat{\Theta}}(t) = -\gamma \Gamma_{kp}^{T}(t) \Phi(\dot{u}(t)) e(t), \quad (13)$$

where γ is a constant, which influences the convergence rate of $\hat{\Theta} \to \Theta$.

3.2. Convergence analysis of neural network with persistent excitation

In this section, we analyze the condition of the convergence of the whole identification system (i.e. $\hat{\Theta} \to \Theta$). The differential equation of the whole identification system is given as

$$\begin{cases} \dot{\tilde{\Theta}}(t) + \gamma \Gamma_{kp}^{T}(t) \Phi(\dot{u}) \Phi^{T}(\dot{u}) \Gamma_{kp}(t) \tilde{\Theta}^{T}(t) = \gamma \Gamma_{kp}^{T}(t) \Phi(\dot{u}) \epsilon \\ e(t) = \Gamma_{kp}^{T}(t) \tilde{\Theta}^{T} \Phi(\dot{u}(t)) - \epsilon, \end{cases} \quad (14)$$

The stability condition of the identification system (14) is obtained via Lemma 2.

Lemma 2. *For making the solution of the homogeneous equation (14) converges to zero in the form of exponentially fast, the $\Gamma_{kp}^{T}(t)\Phi(\dot{u})$ satisfies the persistent excitation condition.*

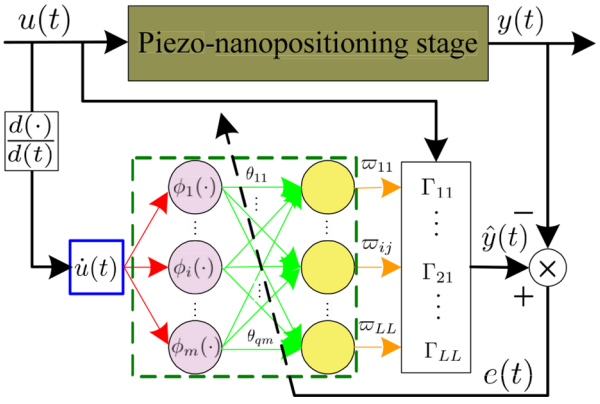

Figure 4. Structure diagram of the RKP model identification process.

$$\dot{\tilde{\Theta}}(t) + \gamma \Gamma_{kp}^{T}(t) \Phi(\dot{u}(t)) \Phi^{T}(\dot{u}(t)) \Gamma_{kp}(t) \tilde{\Theta}^{T}(t) = 0. \quad (15)$$

The persistent excitation condition is explained in Definition 1.

Definition 1. *Gorinevsky (1994) If a piecewise continuous vector $\Xi(t) \in \Re^{N}$ is persistent excitation with a level of excitation $c_1 > 0$, there exists $c_2 > 0, \Delta > 0$, such that*

$$c_2 I \geqslant \int_{t_0}^{t_0 + \Delta} \Xi^{T}(t) \Xi(t) dt \geqslant c_1 I, \forall t \geqslant 0, \quad (16)$$

where c_2 is a constant, $I \in \Re^{N \times N}$ is the identity matrix.

Let us consider the solution of the homogeneous equation (14) as

$$\tilde{\Theta}(t) = \exp\left(-\gamma \int_{0}^{t} \Gamma_{kp}^{T} \Phi(\dot{u}(\tau)) \Phi^{T}(\dot{u}(\tau)) \Gamma_{kp} d\tau \right) \tilde{\Theta}(0), \quad (17)$$

where $\tilde{\Theta}(0) = \hat{\Theta}(0) - \Theta^{\star}$. When $\Gamma_{kp}^{T}(t)\Phi(\dot{u}(t)) = 0$, $\tilde{\Theta}(t)$ cannot approach to zero, a necessary and sufficient condition for $\tilde{\Theta}(t)$ approaches to zero exponentially fast is that $\Gamma_{kp}^{T}(t)\Phi(\dot{u}(t))$ satisfies

$$\int_{t}^{t + \Delta} \Gamma_{kp}^{T} \Phi(\dot{u}(\tau)) \Phi^{T}(\dot{u}(\tau)) \Gamma_{kp} d\tau \geqslant c_2 I, \quad (18)$$

for $\forall\, t \in [0, \infty]$, $\exists\ c_2 > 0, \Delta > 0$ i.e. $\Gamma_{kp}^{T}\Phi(\dot{u}(t))$ is persistent excitation.

Next, we verify that $\Gamma_{kp}^{T}\Phi(\dot{u}(t))$ satisfies the persistent excitation condition. In this study, we assume that $u(t)$ and $\dot{u}(t)$ are persistent excitation. The excitation function ϕ_i of the hidden layer is selected as the Gaussian function. It is easy to obtain that $\Phi(\dot{u}(t))$ is persistent excitation in accordance with Theorem 2 in Gorinevsky (1995). Hence, one of our major work in this section is to prove that Γ_{kp}^{T} is also persistent excitation with the input signal $u(t)$.

The amount of the frequency components of the input signal $u(t)$ must be more than that of unknown parameters. We structure the following input sequence: for any time in sampling time interval, there is the time $T_n \leqslant t_1^- < t_1^+ \cdots < t_i^- < t_i^+ < \cdots \leqslant T_{n+1}$ or $T_n \leqslant \cdots < t_1^+ < t_1^- < t_i^+ < t_i^- < \cdots \leqslant T_{n+1}$, such that $u_i(t^-)$ is the local minimum and $u_i(t^+)$ is the local maximum for each $i \in [1, 2, \cdots, L]$. In addition, $u_i(t^-)$ and $u_i(t^+)$ can include all input values on Preisach plane. If the input signal $u(t)$ satisfies $u(t) < u(t+1)$, Γ_{ij} must exist a local maximum, which is compared with ridge function $r(u(t); \nu_1, \nu_2)$ at this moment; if the input signal $u(t)$ satisfies $u(t+1) < u(t)$, Γ_{ij} must exist a local minimum, which is compared with ridge function $r(u(t); \nu_1, \nu_2)$ at this moment. For each situation, $\zeta(\nu_1, \nu_2)$ will clear and reset the value of each operator at the next moment, which will not lost the excitation information. Therefore, Γ_{kp}^T is persistent excitation with the above input sequence. Because $\Phi(\dot{u}(t))$ and Γ_{kp}^T both satisfy the persistent excitation condition, they are both linearly independent on the interval $[t_0, t_0 + \Delta]$ from the Theorem 2.

Theorem 2. *For $t \in [t_0, t_0 + \Delta]$, $\Xi_i(t)$, $(i = 1, 2, \cdots, N)$ is linearly independent, which is equivalent to that $\Xi(t)$ satisfies $\int_{t_0}^{t_0+\Delta} \Xi^T(t)\Xi(t)dt \geqslant c_2 I$, for $t \in [t_0, t_0 + \Delta]$ and $\exists\, c_2 > 0, \Delta > 0$.*

Proof. We use a contradiction to prove Theorem 2. First, we assume that $\int_{t_0}^{t_0+\Delta} \Xi^T(t)\Xi(t)dt \geqslant c_2 I$, for $t \in [t_0, t_0 + \Delta]$ and $\exists\, c_2 > 0, \Delta > 0$ is true; for $t \in [t_0, t_0 + \Delta]$, $\Xi_i(t)$, $(i = 1, 2, \cdots, N)$ is not linearly independent. Therefore, existing Λ is non-vanishing vector, which satisfies that $\Xi(t)^T \Lambda = 0$, and then,

$$\Lambda^T \left[\int_{t_0}^{t_0+\Delta} \Xi^T(t)\Xi(t)dt \right] \Lambda = \int_{t_0}^{t_0+\Delta} [\Xi^T(t)\Lambda]^2 dt = 0. \quad (19)$$

Because $\int_{t_0}^{t_0+\Delta} \Xi^T(t)\Xi(t)dt \geqslant c_2 I$ $(t \in [t_0, t_0 + \Delta]$ and $\exists\, c_2 > 0, \Delta > 0)$ is true, $\int_{t_0}^{t_0+\Delta} \Xi^T(t)\Xi(t)dt$ must be a positive definite matrix, which is inconsistent with the assumption. Next, assume that $\Xi_i(t)$, $(i = 1, 2, \cdots, N)$, $(t \in [t_0, t_0 + \Delta])$ is linearly independent; and the matrix $\int_{t_0}^{t_0+\Delta} \Xi^T(t)\Xi(t)dt$ is not a positive definite matrix, then existing elements of Λ are not complete zeroes, which make formula (19) true. We can derive that $\Xi(t)^T \Lambda = 0$, which contradicts the assumption.

Because $\Phi(\dot{u}(t))$ and Γ_{kp}^T are both linearly independent on the interval $[t_0, t_0 + \Delta]$, we can obtain that $\Gamma_{\text{kp}}^T \Phi(\dot{u}(t))$ is linearly independent according to the basic mathematics principle. $\Gamma_{\text{kp}}^T \Phi(\dot{u}(t))$ is persistent excitation from the Theorem 2. And then, $\tilde{\Theta}(t)$ approaches to zero exponentially fast.

4. Direct compensation control

In this section, we design a DCC method for the hysteresis of the piezo-nanopositioning stage. The objective of the DCC method is to obtain a desired control voltage signal to drive the piezo-nanopositioning stage, so that the output displacement of the stage can accurately track the desired given signal. The relationship between the compensation KP operator and the KP operator is given as

$$\psi_{\nu_1,\nu_2}[u; \zeta(\nu_1, \nu_2)](t) + \psi^{-1}_{\nu_1,\nu_2}[u; \xi; \zeta_o(\nu_1, \nu_2)](t) = u(t), \quad (20)$$

where $\psi^{-1}_{\nu_1,\nu_2}[u; \xi; \zeta_o(\nu_1, \nu_2)](t)$ represents the compensation KP operator. For convenience, $\psi^{-1}_{\nu_1,\nu_2}[u; \xi; \zeta_o(\nu_1, \nu_2)](t)$ is expressed as $\Upsilon_{\text{kp}}(t)$, which is given as

$$\Upsilon_{\text{kp}}(t) = \begin{cases} \min[u - \xi + \zeta_o(\nu_1, \nu_2), r_o(u - \nu_2) + \nu_2]\, \dot{u}(t) > 0 \\ \max[u - \xi + \zeta_o(\nu_1, \nu_2), r_o(u - \nu_1) + \nu_1]\, \dot{u}(t) \leqslant 0, \end{cases} \quad (21)$$

where $r_o(u; \nu_1, \nu_2)(t)$ is the boundary function, which is defined as

$$r_o(u; \nu_1, \nu_2)(t) = \begin{cases} u(t) & u(t) \in [-\infty, 0] \\ (1 - \nu_{\max}/\sigma) * u(t) & u(t) \in [0, \sigma] \\ u(t) - \nu_{\max} & u(t) \in [\sigma, +\infty], \end{cases} \quad (22)$$

The $(\xi; \zeta_o)$ is the memory turning point of the compensation KP operator, which are defined as follows, respectively

$$\xi(t) = \begin{cases} u(T_0) & t = T_0 \\ u(T_a) & t = T_a \geqslant T_{a-1}, \dot{u}(t)\,\text{sgn}(\dot{u}(t)) < 0 \\ u(T_{a-1}) & t \in [T_{a-1}, T_a], \dot{u}(t)\,\text{sgn}(\dot{u}(t)) \geqslant 0, \end{cases} \quad (23)$$

$$\zeta_o(t) = \begin{cases} \zeta_o(\nu_1, \nu_2)(T_{a-1}) & t \in [T_{a-1}, T_a], \dot{u}(t)\,\text{sgn}(\dot{u}(t)) \geqslant 0 \\ \Upsilon_{\text{kp}}(T_a) & t = T_a \geqslant T_{a-1}, \dot{u}(t)\,\text{sgn}(\dot{u}(t)) < 0 \\ u(T_0) & t = T_0, \end{cases}, \quad (24)$$

It is worth noting that the calculation method of the compensation KP operator is similar with that of KP operator. The only difference is that the maximum and minimum values of the KP operator are counter to that of compensation KP operator when the sign symbol of $\dot{u}(t)$ changes. According to (7) and (20), the following formula is obtained as

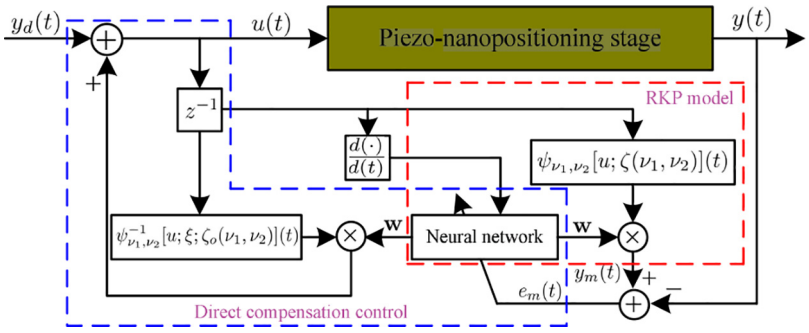

Figure 5. Structure diagram of the DCC method.

$$\begin{aligned} y(t) &= u(t) - \sum_{i=1}^{L}\sum_{j=1}^{i} \Upsilon_{\mathrm{kp}}^{i,j}(t)\varpi_{i,j} \\ &= u(t) - \Upsilon_{\mathrm{kp}}^{T}(t)\mathbf{w}, \end{aligned} \tag{25}$$

where $\Upsilon_{\mathrm{kp}} = [\Upsilon_{11}\,\Upsilon_{21}\,\Upsilon_{22}\,\Upsilon_{31}\cdots\Upsilon_{ij}\cdots\Upsilon_{LL}]^T$, $\varpi_{i,j}$ is the density function, note that the density function of the inverse RKP model is same with that of RKP model, which is obtained using neural network. Based on (25), we get the control law as follow

$$u(t) = y_{\mathrm{d}}(t) + \Upsilon_{\mathrm{kp}}^{T}(t)\mathbf{w}, \tag{26}$$

where $y_{\mathrm{d}}(t)$ is the desired trajectory signal; $u(t)$ represents the control voltage signal. In this paper, the computational error is defined as

$$e_{\mathrm{m}}(t) = y_{\mathrm{m}}(t) - y(t), \tag{27}$$

where $y_{\mathrm{m}}(t)$ is the output of the RKP model. According to (12), we rewrite (27) as

$$e_{\mathrm{m}}(t) = \Gamma_{\mathrm{kp}}^{T}(t)\Theta_{\mathrm{m}}^{T}\Phi(\dot{u}(t)) - y(t). \tag{28}$$

Based on the gradient method, the minimizing trajectory $\Theta_{\mathrm{m}}(t)$ is obtained by

$$\dot{\Theta}_{\mathrm{m}}(t) = -\gamma\Gamma_{\mathrm{kp}}^{T}(t)\Phi(\dot{u}(t))e_{\mathrm{m}}(t). \tag{29}$$

So, the density function of the DCC method is calculated as $\mathbf{w} = \Theta_{\mathrm{m}}^{T}\Phi(\dot{u}(t))$.

Figure 5 is the schematic of the DCC method for hysteresis of the piezo-nanopositioning stage. As shown in Figure 5, $u(t)$ is the obtained control voltage signal. According to (26), $u(t)$ is the sum of $y_{\mathrm{d}}(t)$ and $\Upsilon_{\mathrm{kp}}^{T}(t)\mathbf{w}$. Because the input of $\Upsilon_{\mathrm{kp}}^{T}(t)$ is $u(t)$, we use $u(t-1)$ as its input for avoiding the algebraic loop problem in the control process.

5. Experimental results and discussion

In this section, we give a series of experiments to certify the effectiveness of the created RKP model and DCC method. This section contains three parts: the first part is the introduction of experimental setup; the second part is to test the property of RKP model with different drive signals; the last one is the validation of the proposed DCC method.

5.1. Experimental setup

This paper utilizes a experimental setup to verify the performance of the proposed hysteresis modeling and control method. The experimental setup is composed of the host computer, the precision positioning controller (it includes a resistance strain gauge sensor with a resolution of 5 nm and piezoelectricity ceramic power supply, which is provided by Suzhou Boshi Roboties Technology, China), the piezo-nanopositioning stage (MPT-2MRL102A, Suzhou Boshi Robotics Technology, China), the vibration isolation platform (Sunnylink Precise Machine and Electronics, Wuhan, China) and the data acquisition card (PCI-1716, Advantech, Beijing, China). In the experimental process, the host computer with Matlab software is used to implement the modeling and control method programs. The digital-analog (D/A) and analog-digital (A/D) conversion module is carried out using PCI-1716. The vibration isolation platform avoids the influence of external vibration and noise on the experimental results. The sampling time of the whole systems is set as 0.1 ms. The picture of experimental setup is shown in Figure 6.

5.2. Validation of the RKP model

In this section, to confirm the performance of the proposed RKP model, we use the sinusoid signal with decreasing amplitudes as the driving signal. The frequencies of driving signal are set as 1, 20, and 50 Hz, respectively. To weigh the modeling accuracy associated with the increased the operator number compared with the cost of calculation, we set the operator number as 10; numbers of hidden neurons and output layer neurons are both 13. The property index of modeling results is evaluated via the relative error (RE) and root-mean-square error (RMSE) in a steady state.

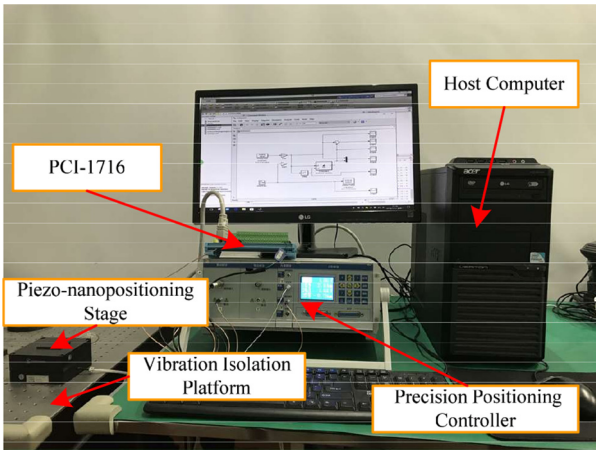

Figure 6. Picture of the experimental setup.

Figures 7 and 8 are the hysteresis modeling results of the piezo-nanopositioning stage for the combination of sinusoid signal with different frequencies. It is obvious that the proposed RKP model can capture the hysteresis nonlinearity of the piezo-nanopositioning stage. As shown in Figures 7(a) and 8(a), the frequency of driving input is 1 Hz, the RKP model output is consistent with the experimental output, and it has a short time to adjust and obtain suitable RKP model output. The RE and RMSE of the RKP model output at 1 Hz are 0.11% and 0.0150 μ m, respectively. Compared with the method in reference (Li et al., 2013), the RMSE of the RKP model is improved by 94.57%. When the frequency of the input driving signal is 20 Hz, the RMSE of the proposed RKP model is decreased by 80.01% compared with the RMSE of the modeling approach proposed by Li et al. (2013). As shown in Figures 7(c) and 8(c), hysteresis modeling error at 50 Hz begins to stabilize after 0.002 s with the RE of 1.85% and RMSE of 0.3502 μ m. Some comparison experimental results are summarized in Table 1. It is noteworthy that proposed RKP model is completely superior to the modeling method proposed by Li et al. (2020). In addition, the modeling errors are increased with the increase of input frequency. The neural network needs enough information to obtain the accurate dynamic density function. However, the information data will decrease with the increase of input frequency. So, the modeling capability is related to the experiment hardware. Note that the modeling error of

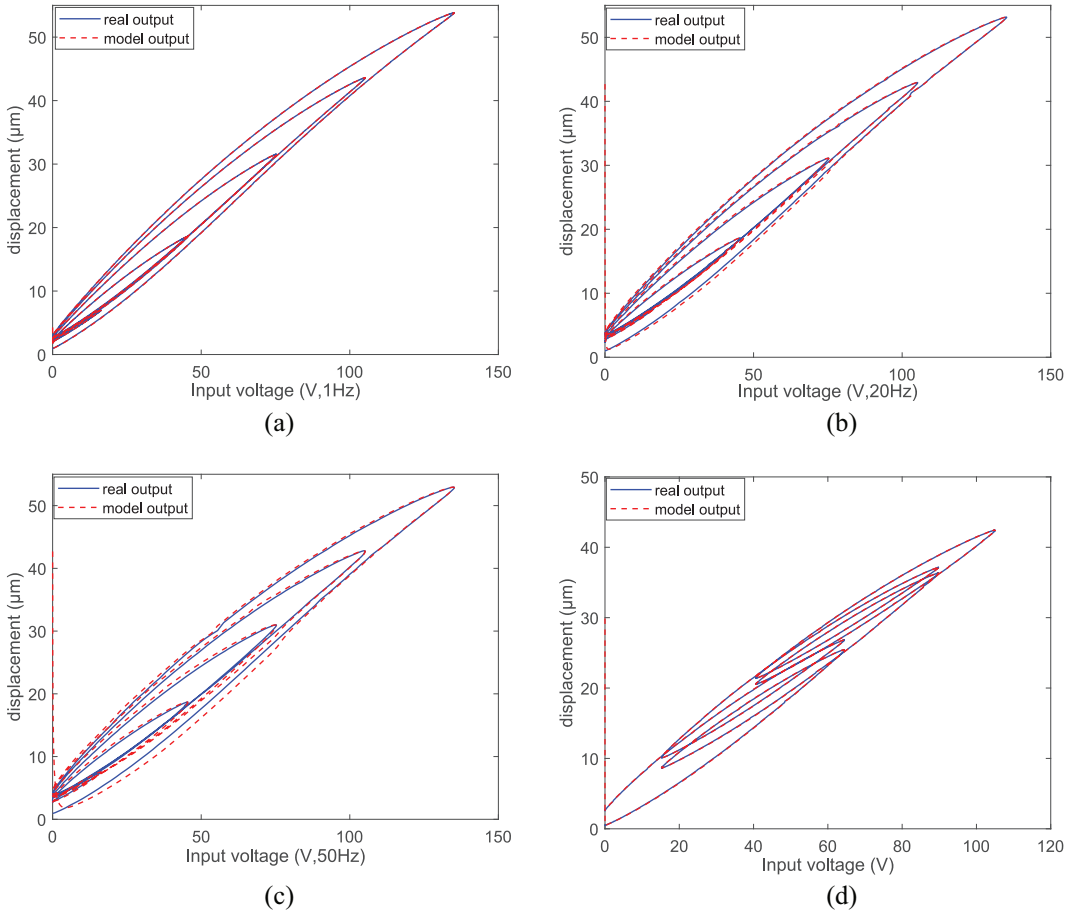

Figure 7. Hysteresis loops modeling results under different sinusoid input voltages: (a) 1 Hz, (b) 20 Hz, (c) 50 Hz, and (d) complex frequency.

Table 1. Modeling performance comparison between model in Li et al. (2020) and proposed RKP model.

Input type (frequency)	RKP model (RMSE/RE, μ m/%)	Model in Li et al. (2020) (RMSE/RE, μ m/%)
f = 1 Hz	0.0150/0.11	0.2761/0.80
f = 20 Hz	0.1443/0.93	0.7219/2.08
f = 50 Hz	0.3502/1.85	1.0543/3.04
f = 1*5 Hz	0.0196/0.23	0.7065/3.83

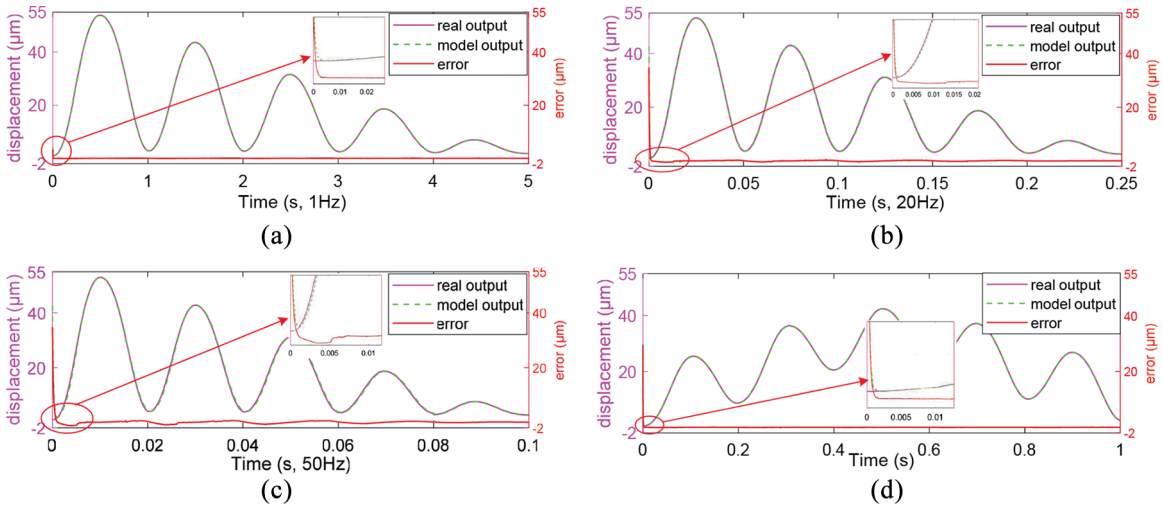

Figure 8. Hysteresis modeling results under different sinusoid input voltages: (a) 1 Hz, (b) 20 Hz, (c) 50 Hz, and (d) complex frequency.

the RKP model is recorded as ± 0.3502 μ m for less than 50 Hz input signal. Finally, we use the complex sine signal (i.e. $u = 22.5\sin(10\pi t - 0.5\pi) + 15\sin(2\pi t - 0.5\pi) + 37.5$) as the driving signal to identify the density function of the proposed RKP model. Figures 7(d) and 8(d) illustrate that the proposed RKP model can precisely describe the hysteresis loop with multi-minor loops of the piezo-nanopositioning stage; the RE and RMSE are 0.23% and 0.0196 μ m, respectively. It proves the superior performance of the proposed RKP model.

6. Controller performance evaluation

To certify the performance of the DCC method, we use the triangular signal as the desired trajectory signal to carry out the trajectory tracking experiments. In these tracking experiments, the number of the inverse KP operator is also 10; the structure of the neural network in the DCC method is similar to the RKP model. Figure 9 illustrates the tracking performance of the piezo-nanopositioning stage under the ramp desired signal with different γ. The solid blue line Ref. is the desired signal; it is obvious that when $\gamma = 0.8$, the system has the minimum settling time and overshoot. In

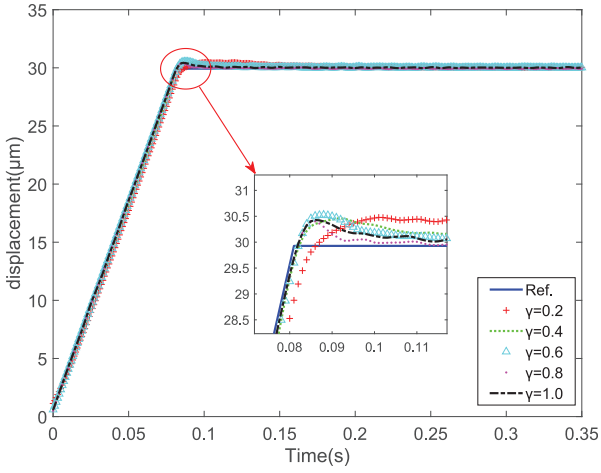

Figure 9. Tracking performance of the piezo-nanopositioning stage with different γ.

the follow-up tracking experiment, γ is set as 0.8 to obtain the appropriate $\mathbf{w}$ using the neural network.

The experiments for the desired trajectory signal that is associated with the triangular trajectory signal (1, 10, and 50 Hz) are carried out. Figures 10 to 12 show that the actual displacement of the piezo-nanopositioning

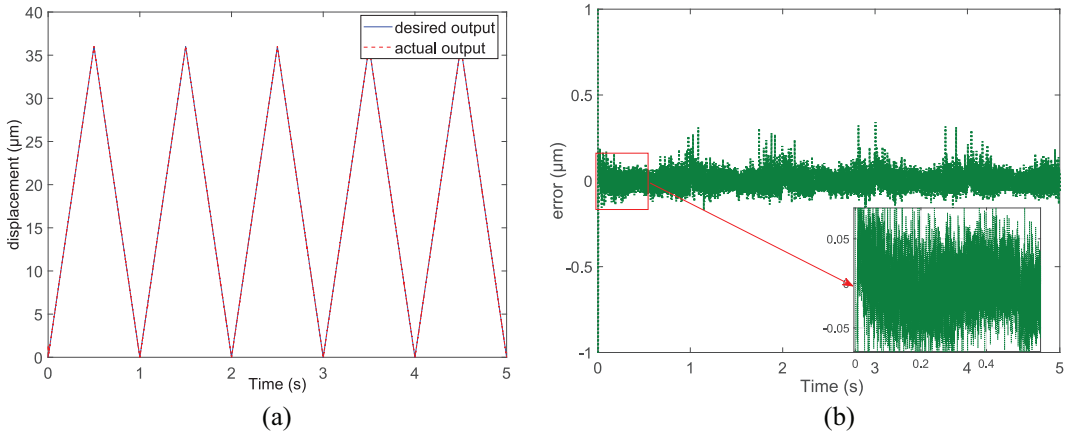

Figure 10. Tracking results for the 1 Hz triangular signal: (a) comparison between the desired and actual outputs and (b) tracking error.

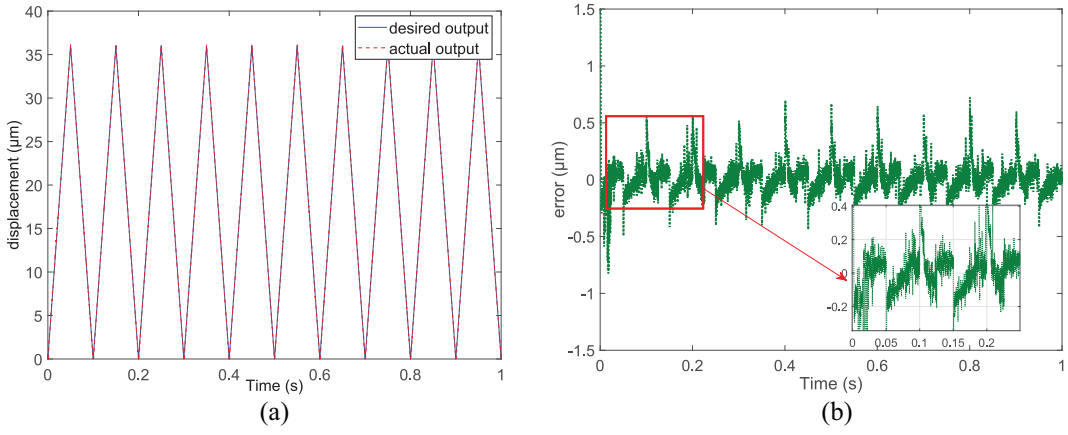

Figure 11. Tracking results for the 10 Hz triangular signal: (a) comparison between the desired and actual outputs and (b) tracking error.

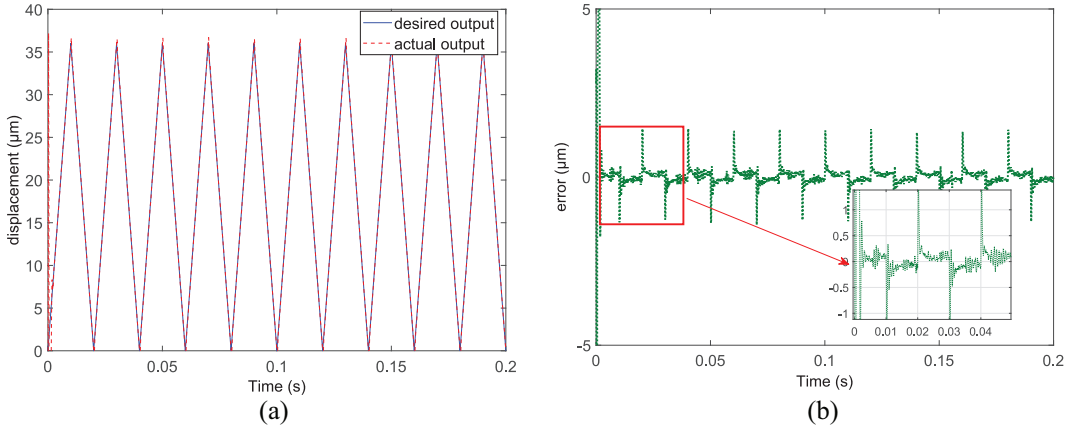

Figure 12. Tracking results for the 50 Hz triangular signal: (a) comparison between the desired and actual outputs and (b) tracking error.

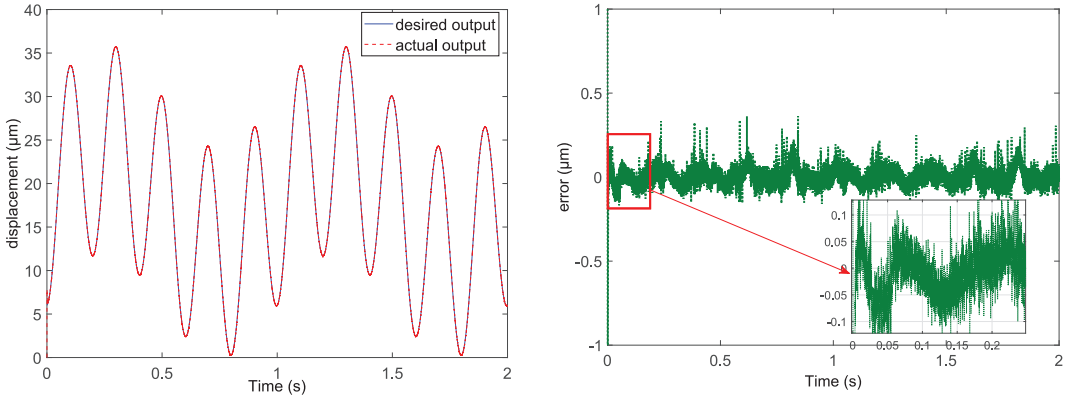

Figure 13. Tracking results for the complex harmonic signal: (a) comparison between the desired and actual outputs and (b) tracking error.

Table 2. Comparison of performance between controller in Xu et al. (2018) and proposed DCC method.

Input type (frequency)	Proposed DCC method (AME/RMSE, μ m)	Existing controller (AME/RMSE, μ m)
f = 1 Hz	0.0273/0.0464	0.0549/0.0695
f = 10 Hz	0.0891/0.1138	0.1190/0.1327
f = 50 Hz	0.1489/0.2518	———/———
f = 1*5 Hz	0.0370/0.0478	0.1087/0.1263

stage tracks the desired trajectory signal well. When the frequency is less than 50 Hz, the tracking error at steady state based on the DCC method is reduced into less than 1.4282 μ m. In Figure 13, the complex harmonic signal (i.e. $y_d(t) = 12\sin(2\pi t - 0.5\pi) + 6\sin(10\pi t) + 18$) is used as the desired trajectory signal, the experimental result shows the proposed DCC method can still achieve good control effect for a given signal with frequency variation.

In order to further illustrate the superior performance of the DCC method, the results of the comparative experiments (compared with the sliding mode control with perturbation estimation (SMCPE) method proposed by Xu et al. (2018) are summarized in Table 2. For the 10 Hz trajectory signal, the absolute mean error (AME) and RMSE of the DCC method are reduced by 25.13% and 14.24% in compared with that of SMCPE method. For the complex harmonic signal, the DCC method generates 65.96% lower AME tracking error and 62.15% lower RMSE tracking error than SMCPE method.

In addition, compared with the existing literature (Li et al., 2018; Pan et al., 2019), the experimental results show that the proposed DCC method can not only effectively reduce the computational burden, but also improve the control precision of the piezo-nanopositioning stages. This mainly comes from the fact that the dynamic density function of the DCC method can be obtained in real time way using neural network.

7. Conclusion

This paper mainly focuses on the modeling and the DCC of the hysteresis in piezo-nanopositioning stages. A RKP model is used to capture the rate-dependent hysteresis of the piezo-nanopositioning stage. The convergence of the neural network with the KP operators is demonstrated under the persistent exciting conditions. From experimental results, it is clear that the neural network is convergent and the RKP model has better results than the rate-dependent Bouc-Wen model in the aspect of describing the rate-dependent hysteresis in piezo-nanopositioning stages. A DCC method is presented to mitigate the hysteresis in piezo-nanopositioning stages. For the complex harmonic signal, the AME and RMSE of the proposed DCC method are reduced by more than 60% compared with that of the SMCPE method. In the future, the proposed DCC method will be further improved to extend for the application in high-precision positioning control fields.

Declaration of conflicting interests

The authors declared no potential conflicts of interest with respect to the research, authorship, and/or publication of this article.

Funding

The authors disclosed receipt of the following financial support for the research, authorship, and/or publication of this article: This study was supported in part by Program of Science and Technology Development Plan of Jilin Province of China (20180101052JC, 20190303020SF); The China Postdoctoral Science Foundation (2020TQ0350).

ORCID iD

Rui Xu https://orcid.org/0000-0002-8040-2768

References

Al Janaideh M and Krejci P (2012) Inverse rate-dependent Prandtl-Ishlinskii model for feedforward compensation of hysteresis in a piezomicropositioning actuator. *IEEE/ASME Transactions on Mechatronics* 18(5): 1498–1507.

Al Janaideh M, Saaideh M and Rakotondrabe M (2020) On hysteresis modeling of a piezoelectric precise positioning system under variable temperature. *Mechanical Systems and Signal Processing* 145: 106880.

Al Janaideh M, Xu R and Tan X (2021) Adaptive estimation of play radii for a Prandtl-Ishlinskii hysteresis operator. *IEEE Transactions on Control Systems Technology*. Epub ahead of print 2021. DOI: 10.1109/TCST.2020.3046019.

Chen J, Ren B and Zhong Q (2016) UDE-based trajectory tracking control of piezoelectric stages. *IEEE Transactions on Industrial Electronics* 63(10): 6450–6459.

Dong R, Tan Y and Xie Y (2016) Identification of micropositioning stage with piezoelectric actuators. *Mechanical Systems and Signal Processing* 75: 618–630.

Gorinevsky D (1994) On the persistency of excitation in RBF network identification. In: *Proceedings of 1994 american control conference (ACC)*, Baltimore, MD, USA, 29 June–1 July 1994, pp.1442–1443. New York: IEEE.

Gorinevsky D (1995) On the persistency of excitation in radial basis function network identification of nonlinear systems. *IEEE Transactions on Neural Networks* 6(5): 1237–1244.

Guo Y, Mao J and Zhou K (2015) Rate-dependent modeling and H_∞ robust control of GMA based on Hammerstein model with Preisach operator. *IEEE Transactions on Control Systems Technology* 23(6): 2432–2439.

Hu H, Georgiou HM and Ben-Mrad R (2005) Enhancement of tracking ability in piezoceramic actuators subject to dynamic excitation conditions. *IEEE/ASME Transactions on Mechatronics* 10(2): 230–239.

Iyer RV, Tan X and Krishnaprasad PS (2005) Approximate inversion of the Preisach hysteresis operator with application to control of smart actuators. *IEEE Transactions on Automatic Control* 50(6): 798–810.

Kuhnen K and Krejci P (2009) Compensation of complex hysteresis and creep effects in piezoelectri-cally actuated systems-a new Preisach modeling approach. *IEEE Transactions on Automatic Control* 54(3): 537–550.

Li W, Chen X and Li Z (2013) Inverse compensation for hysteresis in piezoelectric actuator using an asymmetric rate-dependent model. *Review of Scientific Instruments* 84(11): 115003.

Li W, Nie L, Liu Y, et al. (2020) Rate dependent Krasnoselskii-Pokrovskii modeling and inverse compensation control of piezoceramic actuated stages. *Sensors* 20(18): 5062.

Li Z, Shan J and Gabbert U (2018) Inverse compensation of hysteresis using Krasnoselskii-Pokrovskii model. *IEEE/ASME Transactions on Mechatronics* 23(2): 966–971.

Liu Y, Gao X and Li Y (2016) Giant magnetostrictive actuator nonlinear dynamic Jiles-Atherton model. *Sensors and Actuators A: Physical* 250: 7–14.

Nguyen ML, Chen X and Yang F (2018) Discrete time quasi sliding mode control with prescribed performance function and its application to piezo-actuated positioning systems. *IEEE Transactions on Industrial Electronics* 65(1): 942–950.

Pan W, Xu R and Zhou M (2019) Modeling of hysteresis for piezo-driven stages using a rate-dependent Krasnosel'skii-Pokrovskii model. In: *2019 Chinese Control Conference (CCC)*, Guangzhou, China, 27–30 July 2019, pp.1604–1609. New York: IEEE.

Song G, Zhao J, Zhou X, et al. (2005) Tracking control of a piezoceramic actuator with hysteresis compensation using inverse Preisach model. *IEEE/ASME Transactions on Mechatronics* 10(2): 198–209.

Tan X and Baras JS (2005) Adaptive identification and control of hysteresis in smart materials. *IEEE Transactions on Automatic Control* 50(6): 827–839.

Visintin A (2013) *Differential Models of Hysteresis*. Berlin: Springer Science and Business Media.

Wang H, Liu P and Liu S (2017) Adaptive neural synchronization control for bilateral teleoperation systems with time delay and backlash-like hysteresis. *IEEE Transactions on Cybernetics* 47(10): 3018–3026.

Webb GV, Lagoudas DC and Kurdila AJ (1998) Hysteresis modeling of SMA actuators for control applications. *Journal of Intelligent Material Systems and Structures* 9(6): 432–448.

Xiao S and Li Y (2012) Modeling and high dynamic compensating the rate-dependent hysteresis of piezoelectric actuators via a novel modified inverse Preisach model. *IEEE Transactions on Control Systems Technology* 21(5): 1549–1557.

Xu R and Zhou M (2017a) Sliding mode control with sigmoid function for the motion tracking control of the piezo-actuated stages. *Electronics Letters* 53(2): 75–77.

Xu R and Zhou M (2017b) Elman neural network-based identification of Krasnosel'skii-Pokrovskii model for magnetic shape memory alloys actuator. *IEEE Transactions on Magnetics* 53(11): 2002004.

Xu R, Zhang X, Guo H, et al. (2018) Sliding mode tracking control with perturbation estimation for hysteresis nonlinearity of piezo-actuated stages. *IEEE Access* 6: 30617–30629.

Yang M, Li C, Gu G, et al. (2015) Modeling and compensating the dynamic hysteresis of piezoelectric actuators via a modified rate-dependent Prandtl-Ishlinskii model. *Smart Materials and Structures* 24(12): 125006.

Yu Y, Zhang C, Wang Y, et al. (2021) Neural network-based iterative learning control for hysteresis in magnetic shape memory alloy actuator. *IEEE/ASME Transactions on Mechatronics*. Epub ahead of print 2021. DOI: 10.1109/TMECH.2021.3075057.

Zhang J, Merced E, Sepulveda N, et al. (2015) Optimal compression of generalized Prandtl-Ishlinskii hysteresis models. *Automatica* 57: 170–179.

Zhang X, Wang Y, Wang C, et al. (2019) Adaptive estimated inverse output-feedback quantized control for piezoelectric positioning stage. *IEEE Transactions on Cybernetics* 49(6): 2106–2118.

Zhou M, Yang P, Wang J, et al. (2016) Adaptive sliding mode control based on duhem model for piezoelectric actuators. *IETE Technical Review* 33(5): 557–568.